Volume 14
Number 7
27 January 2026
Pages 3705–4290

Journal of Materials Chemistry A

Materials for energy and sustainability

rsc.li/materials-a

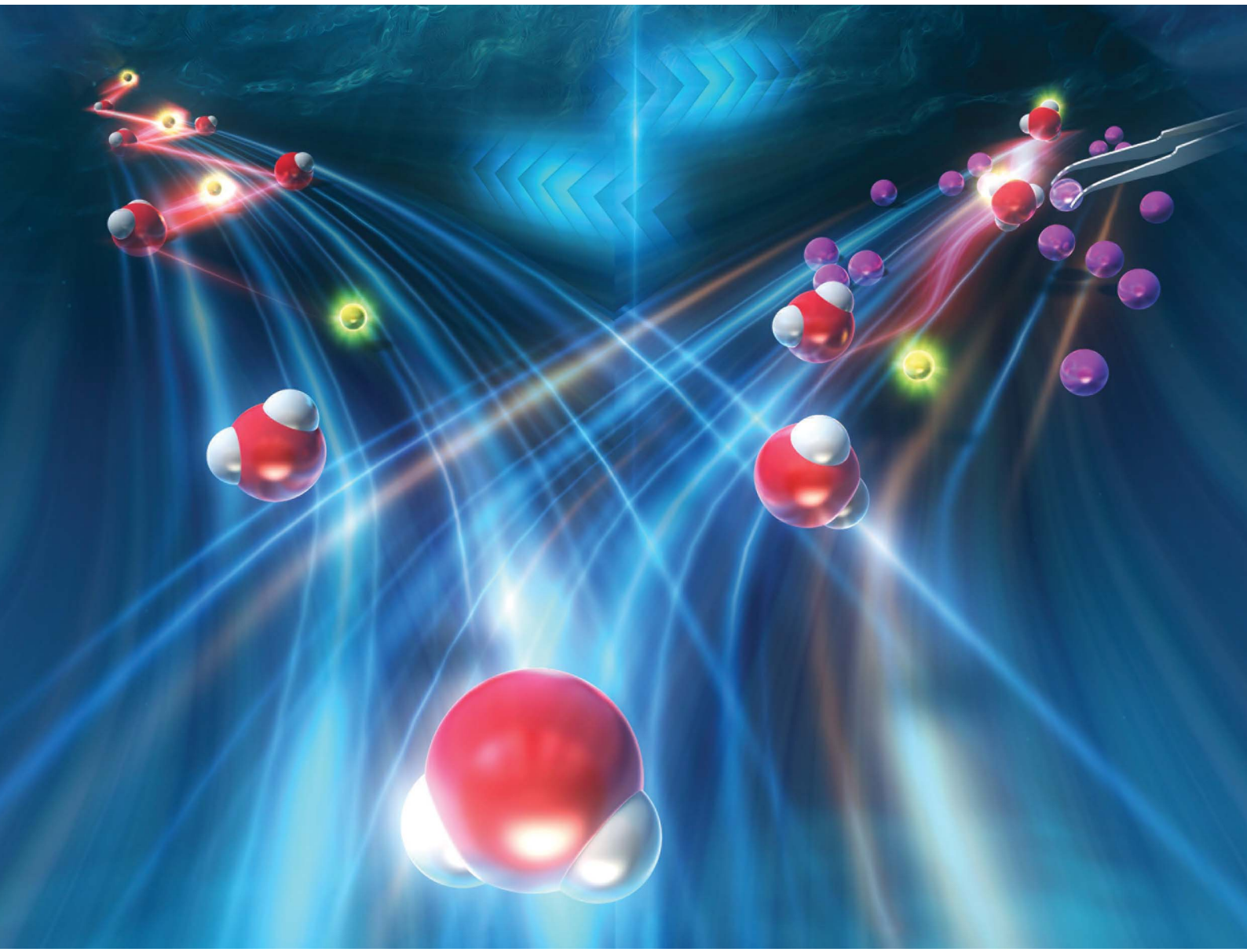

ISSN 2050-7488

ROYAL SOCIETY OF CHEMISTRY

PAPER

Kouki Oka, Tatsuo Kimura *et al.*

Proton conductivity at the controlled hydrophilic and hydrophobic surfaces of mesoporous aluminum organophosphonates

Journal of Materials Chemistry A

ROYAL SOCIETY OF CHEMISTRY

PAPER

View Article Online
View Journal | View Issue

Cite this: J. Mater. Chem. A, 2026, 14, 3863

Proton conductivity at the controlled hydrophilic and hydrophobic surfaces of mesoporous aluminum organophosphonates

Takahiro Ami,[a] Kouki Oka, *[abc] Hitoshi Kasai[a] and Tatsuo Kimura *[d]

Aluminum organophosphonate (AOP)-type mesoporous materials can be prepared using amphiphilic organic compounds in which an aluminophosphate (AlPO)-based inorganic unit and a designable organic linker are distributed alternately in non-silica-based inorganic–organic hybrid frameworks around supramolecular-mediated mesopores. In general, the resultant AlPO-based frameworks are amorphous and have potential as proton conductive surfaces due to the presence of abundant free phosphoric acid (P–OH) groups and water (H_2O) molecules coordinated to the tetrahedral AlO_4 units in combination with the smooth transportation of protons inside the mesopores. In this study, a series of AOP-type mesoporous materials was prepared using a polymeric triblock copolymer (*e.g.*, Pluronic P123, $EO_{20}PO_{70}EO_{20}$) to reveal the derived proton conductivity at AlPO-based surfaces with and without methylene ($-CH_2-$), ethylene ($-C_2H_4-$) and phenylene ($-C_6H_4-$) groups. The networking of H_2O molecules was restricted by the presence of strongly hydrophobic organic linkers, even under high-humidity conditions (95% RH). This was a key factor to change the proton conductive mechanism from the Vehicle mechanism at low temperature to the Grotthuss mechanism at higher temperature, with a highest proton conductivity of $>10^{-3}$ S cm^{-1}, comparable to that observed for hydrophilic AlPO-based frameworks. The activation energy was negatively proportional to the size of the organic linker due to the decrease in the number of hydrogen bonds formed/broken during the proton conduction. These insights are quite unique for controlling the proton/water transport rate and the mechanism by designing the organic linker of AOP-type mesoporous materials.

Received 28th August 2025
Accepted 13th October 2025

DOI: 10.1039/d5ta06982c

rsc.li/materials-a

1. Introduction

Proton conductive materials are essential for developing a wide variety of cutting-edge electrochemical devices, such as fuel cells, sensors and supercapacitors.[1–3] In general, protons are transported and transferred by using acidic functional groups (*e.g.*,–SO_3H) as well as surface hydroxyl (–OH) ones and/or water (H_2O) molecules adsorbed on the surfaces. Considering such structural features, metal phosphates are one of the promising and highly designable proton conductive materials. As a typical example, aluminophosphate (AlPO)-based materials, structured by alternate tetrahedral AlO_4 and PO_4 units, are very fascinating because of the presence of many P–OH groups and adsorbed H_2O molecules.[4] However, the presence of surface –OH groups is quite limited by the formation of neutral frameworks with alternative networks formed by positive $P^{5+}(O^{2-})_2$ (PO_4) and negative $Al^{3+}(O^{2-})_2$ (AlO_4) in the resultant open-framework AlPO-based materials. In this context, layered AlPO-based materials have so far been introduced as excellent proton conductors due to the presence of many terminal –OH groups and P=O units.[5–8] Besides, most of the previous works are concerned with the optimization of external factors, such as the conditions of measurement (*e.g.*, temperature and humidity) and the type of proton carrier.[9] To improve the proton conductivity by structural design, high-surface-area AlPO-based materials, especially surfactant-assisted mesoporous ones, are quite promising for the formation of amorphous frameworks.

The synthetic approach of mesoporous AlPO-based materials was initially found using alkyltrimethylammonium (C_nTMA)-type surfactant.[10,11] The surface properties of the resultant amorphous frameworks were extremely hydrophilic, which can be revealed by H_2O adsorption–desorption measurements.[12] The use of amphiphilic organic compounds such as EO_nPO_m-EO_n was also possible for the mesostructural design of metal phosphates, including AlPO-based materials.[13–15] In addition to the presence of many P–OH groups, proton carriers like H_2O can be condensed inside continuous channels.[16,17] Accordingly,

[a]Institute of Multidisciplinary Research for Advanced Materials, Tohoku University, 2-1-1 Katahira, Aoba-ku, Sendai, Miyagi 980-8577, Japan. E-mail: oka@tohoku.ac.jp
[b]Carbon Recycling Energy Research Center Ibaraki University, 4-12-1 Nakanarusawa, Hitachi, Ibaraki 316-8511, Japan
[c]Deuterium Science Research Unit, Center for the Promotion of Interdisciplinary Education and Research Kyoto University, Sakyo-ku, Yoshida, Kyoto 606-8501, Japan
[d]National Institute of Advanced Industrial Science and Technology (AIST), Moriyama-ku, Sakurazaka, Nagoya 463-8560, Japan. E-mail: t-kimura@aist.go.jp

porous materials have been studied increasingly for the design of proton conductive devices.[18–20] Acidic functional groups, such as carboxyl (–COOH), sulfonic ($–SO_3H$) and phosphoric ($–PO(OH)_2$) groups, also assist the formation of a hydrogen-bonding network as the proton conduction pathway.[21–23] A wide variety of open-framework materials with designable organic linkers have been investigated to adjust the surface affinity to proton carriers.[24,25] Well-defined AlPO-based materials are very helpful for discussing the effect of structural features on the proton conductivity and the mechanism, rather than amorphous materials like conventional polymers.[26]

So far, we have reported the synthesis of surfactant-assisted mesoporous metal bisphosphonates, mainly aluminum organophosphonate (AOP), as successful examples of inorganic–organic hybrid mesoporous materials.[27,28] The AlPO-based inorganic units are distributed throughout the whole hybrid framework with covalently bonded organic linkers around supramolecular-mediated mesopores. The strong hydrophilicity of the AlPO-based frameworks is reduced by the presence of integral organic groups.[29] The mesostructural parameters (*e.g.*, pore size and wall thickness) of the AlPO-based frameworks can be adjusted without changing the framework composition. This is one of their unique structural features, being totally different from highly crystalline and porous materials such as metal–organic frameworks (MOF) and covalent–organic frameworks (COF).[30,31] The controllable surface properties, in addition to the presence of surfactant-assisted mesopores, are also useful for investigating the proton conductive mechanism due to the presence of free P–OH groups enhanced by the presence of H_2O molecules at the surfaces and/or improving the proton conductivity. In this study, we constructed the molecular-scale structure of AlPO-based frameworks to demonstrate the uniqueness of the amorphous frameworks with many surface P–OH groups. After evaluating the proton conductivity over the designed surfaces containing identical mesopores under the conditions of controlled humidity at different temperatures, we will then discuss the rational guidelines for improving the proton conductivity over AlPO-based frameworks with and without organic linkers.

2. Experimental section

2.1 Materials

Pluronic P123 ($EO_{20}PO_{70}EO_{20}$) was obtained from Sigma-Aldrich. Methylene diphosphonic acid ($(HO)_2OPCH_2PO(OH)_2$) and ethylene diphosphonic acid ($(HO)_2OPC_2H_4PO(OH)_2$) were purchased from AZmax Co. Ltd. Tetraethyl 4,4′-phenylenebisphosphonate ($(H_5C_2O)_2OP\text{-}Ph\text{-}PO(OC_2H_5)_2$) was purchased from Epsilon Chemie. Anhydrous aluminum chloride ($AlCl_3$) and dehydrated ethanol (EtOH) were obtained from Wako Chemical Co. Phosphoric acid (85% H_3PO_4) was purchased from Kanto Chemical Co. Inc.

2.2 Synthesis of mesoporous AOP-type materials

Referring to the key process disclosed in our previous works,[32,33] clear precursor solutions containing Pluronic P123 were prepared for the synthesis of mesoporous aluminum methylene (–CH_2–, –Me–), ethylene (–C_2H_4–, –Et–) and phenylene(–C_6H_4–, –Ph–)bisphosphonate-type materials, respectively expressed as AOP-Me, AOP-Et and AOP-Ph. Although mesoporous AOP-Me- and AOP-Et-type materials were obtained by the reactions between the corresponding bisphosphonic acid and $AlCl_3$,[33] a reactivity-designed phenylene bisphosphonate compound should be used for obtaining the mesoporous AOP-Ph-type one because of an insufficient reactivity of phenylene bisphosphonic acid to $AlCl_3$. An ester-type phenylene bisphosphonate ($(H_5C_2O)_2OP\text{-}Ph\text{-}PO(OC_2H_5)_2$) (17.51 g, 50 mmol) was treated in a closed bottle with an aqueous solution of hydrochloric acid (5 M HCl 20 mL, plus H_2O 20 mL) at around 90 °C for 6 h and dried by heating it in an open Petri dish.[32]

In the synthesis of AOP-Me, AOP-Et and AOP-Ph, all the precursor solutions were prepared by using the same procedure. Pluronic P123 (1.6 g) was dissolved in EtOH (10 mL) containing a little H_2O (1 mL). Anhydrous $AlCl_3$ powder (0.67 g) was added little-by-little to another ethanolic solution (10 mL with H_2O 1 mL) of $(HO)_2OPCH_2PO(OH)_2$ (0.88 g), $(HO)_2OPC_2H_4PO(OH)_2$ (0.96 g) and partly acidified $(H_5C_2O)_2OP\text{-}Ph\text{-}PO(OC_2H_5)_2$ (1.47 g), stirred for 15 min and combined with the ethanolic solution of Pluronic P123. The precursor solutions were stirred for 120 min and spray-dried at 110 °C (Yamato Scientific Co., Spray Dryer GB22). For comparison, a mesoporous AlPO-type material (without organic linkers) was also synthesized through a similar spray drying process.[33] After 85% phosphoric acid (0.33 mL) was added to EtOH (30 mL) containing Pluronic P123 (1.0 g), anhydrous $AlCl_3$ (0.67 g) was added slowly under stirring. After stirring for 30 min, the precursor solution was spray-dried at 170 °C. To remove $EO_nPO_mEO_n$-type amphiphilic organic molecules, all the powder samples (1.5 g) were treated three times in dehydrated acetone at 90 °C for around 16 h in a Teflon tube.[33]

2.3 Characterization

Low-angle X-ray diffraction (XRD) patterns were measured by using a Rigaku RINT 2100 diffractometer with monochromated Fe Kα radiation (40 kV, 30 mA). Fourier transform infrared (FT-IR) spectra were recorded on an IRSpirit spectrophotometer (Shimadzu, Japan). Adsorption–desorption isotherms of nitrogen (N_2) and water (H_2O) vapor were measured at −196 °C and 25 °C by using a BELSORP-max X (MicrotracBEL, Japan), respectively. The samples were degassed at 80 °C for 3 h under vacuum before the measurements. Specific surface area was calculated by the Brunauer–Emmett–Teller (BET) method using adsorption data of N_2 (described as N_2-S_{BET}) and the total pore volume was estimated by using the amount adsorbed at around $P/P_0 = 0.95$. The surface hydrophilicity and hydrophobicity were briefly evaluated by using adsorption behavior and capacity of H_2O molecules.

Proton conductivity was measured by using pelletized samples pressed in a cylindrical die (surface area; 0.785 cm^2). All the samples were pressed under the same conditions with a constant pressure (30 MPa) for 10 s to form their uniform pellets. The compacity of each disk-shaped pellet was 1.41–

1.43 g cm^{-3} and standardized with the thickness of 0.5–1.0 mm. AC impedance measurements were performed with an ALS 760E dual electrochemical analyzer (BAS Ltd) in the frequency range from 10^{-1} to 10^{6} Hz at 0.01 V (amplitude voltage). Relative humidity (RH) and temperature were controlled by an IW223 incubator (Yamato Scientific Co). The resistance value was determined from the equivalent circuit fit (see Fig. S1) of the first semi-circle using pyZwx. The activation energy for proton transport was calculated from the variable temperature data at constant relative humidity (95% RH) using the Arrhenius equation $\sigma = (\sigma_0/T)\exp(-E_a/kT)$, where σ is conductivity, σ_0 is a pre-exponential factor, T is temperature, k is the Boltzmann constant, and E_a is the activation energy. All conductivity values were calculated from the resistance values obtained from three repeated measurements under the same conditions. Protons are conducted by either the Vehicle or the Grotthuss mechanism. The contribution of the Vehicle mechanism increases with E_a of >0.4 eV, whereas that of the Grotthuss mechanism increases with E_a of <0.4 eV.

3. Results & discussion

A series of AOP-type mesoporous materials containing organic linkers, such as ethylene (–CH_2–, –Me–), ethylene (–C_2H_4–, –Et–) and phenylene (–C_6H_4–, –Ph–) groups, were prepared using Pluronic P123 for systematic control of the hydrophilicity and hydrophobicity of the mesopore surfaces. This property can be confirmed through adsorption measurements of H_2O vapor. The AOP-type materials (respectively expressed as AOP-Me, AOP-Et and AOP-Ph) as well as the AlPO-type one (expressed as AlPO without any organic linkers) were then obtained using Pluronic P123 through an evaporation-induced self-assembly (EISA) process by spray-drying the precursor solutions and subsequent treatment in dehydrated acetone to eliminate $EO_nPO_mEO_n$-type amphiphilic organic molecules.

3.1. Aerosol-assisted synthesis of mesoporous AOP-type materials

The FT-IR spectra of the mesoporous AOP-type materials after spray-drying (before the removal of Pluronic P123) and subsequent treatment in dehydrated acetone (after the removal of Pluronic P123) are shown in Fig. 1a, along with those observed for an AlPO-type material. Assignments of the characteristic bands unique to the presence of $EO_nPO_mEO_n$-type amphiphilic organic molecules and the formation of AlPO-based frameworks are summarized in Table S1. For a typical example, the FT-IR spectrum of AOP-Me showed a strong band at 1088 cm^{-1}, which was derived from the vibration of P═O stretching in free phosphate groups.[34,35] The bands at 928–807 cm^{-1} and 561–443 cm^{-1} were ascribed to the vibrations of asymmetric and symmetric Al–O–P stretching, respectively.[34] In addition to those bands, bands due to the presence of $EO_nPO_mEO_n$-type amphiphilic organic compounds were detected at 3009–2893 cm^{-1}, 1638 cm^{-1} and 1450–1372 cm^{-1} before the removal of Pluronic P123, though some of them overlapped with the bands arising from the AlPO-based framework. The broad bands at 3147 cm^{-1} and 1638 cm^{-1} were assignable to the vibrations of O–H stretching and O–H bending in free phosphoric acid (P–OH and P═O) and hydroxy (–OH) groups in Pluronic P123 and adsorbed H_2O.[36] The bands at 3009–2893 cm^{-1} and 1450–1372 cm^{-1} were attributed to the vibrations of C–H stretching and C–H bending in the –CH_2– linkers and Pluronic P123.[35] The bands due to the C–O stretching vibration in Pluronic P123 were included in the range of the P═O stretching vibration (1088 cm^{-1}) (see Fig. S2). The FT-IR spectra of AOP-Et and AlPO exhibited bands due to the AlPO-based framework and Pluronic P123 in almost the same region as in the case of AOP-Me. In addition to those bands, two bands appeared at 1338 cm^{-1} and 1151 cm^{-1} in the FT-IR spectrum of AOP-Ph, which originated from C–H and C═C stretching vibrations of the aromatic ring, respectively.[37] After the removal of Pluronic P123, the bands related to the presence of Pluronic P123 disappeared in all of the spectra. In the case of AOP-Ph, the bands due to the C–H stretching vibration were observed at 2974–2905 cm^{-1}. This is because the ester group of the starting bisphosphonate still remained in part even after completing all the synthetic process (*e.g.*, the preparation of the precursor solution, spray-drying of the precursor solution and subsequent treatment of the dehydrated acetone).

The N_2 adsorption–desorption isotherms and corresponding pore size distribution curves of all the samples are shown in Fig. 1b. All of the isotherms showed type IV behaviors typical for the presence of many mesopores.[38] The pore size distributions were very narrow and centered at around 8.1 nm, indicating the formation of uniform tubular mesopores. For example, the specific surface area and total pore volume of AOP-Me were 357 m^2 g^{-1} and 0.454 cm^3 g^{-1}, respectively. The low-angle XRD patterns of AOP-Me, AOP-Et and AOP-Ph-type mesoporous materials after the removal of Pluronic P123 are shown in Fig. 1c. The *d*-spacings were calculated to be around 9 nm, which were observed at $2\theta = 1.29°$ (8.6 nm) for AOP-Me, 1.26° (8.8 nm) for AOP-Et, 1.24° (9.0 nm) for AOP-Ph and 1.22° (9.1 nm) for AlPO. Higher order diffraction was also detected for each sample (see Fig. S3), but the peaks were very weak, broad and not assignable to a well-ordered mesoporous structure (*e.g.*, the 2-d hexagonal arrangement of cylindrical mesopores).[33] This could be related to the disordered packing of tubular but uniform (8.1 nm) mesopores, being typically observed for surfactant-assisted mesoporous materials inside spray-dried spherical particles. To understand the final mesoporous structure, schematic illustrations of mesoporous AOP-Me-, AOP-Et- and AOP-Ph-type materials, along with that of the mesoporous AlPO-type one, are also provided in Fig. 1c.

3.2. Surface properties of the AOP-type mesoporous materials

The H_2O adsorption–desorption isotherms of the AOP-Me, AOP-Et, AOP-Ph and AlPO-type mesoporous materials are shown in Fig. 2a. The isotherm of AOP-Me seemed to be type IV; the adsorption of H_2O molecules started at the low range of relative humidity (RH) and increased gradually with capillary condensation at around $P/P_0 = 0.5$. A large hysteresis loop was also

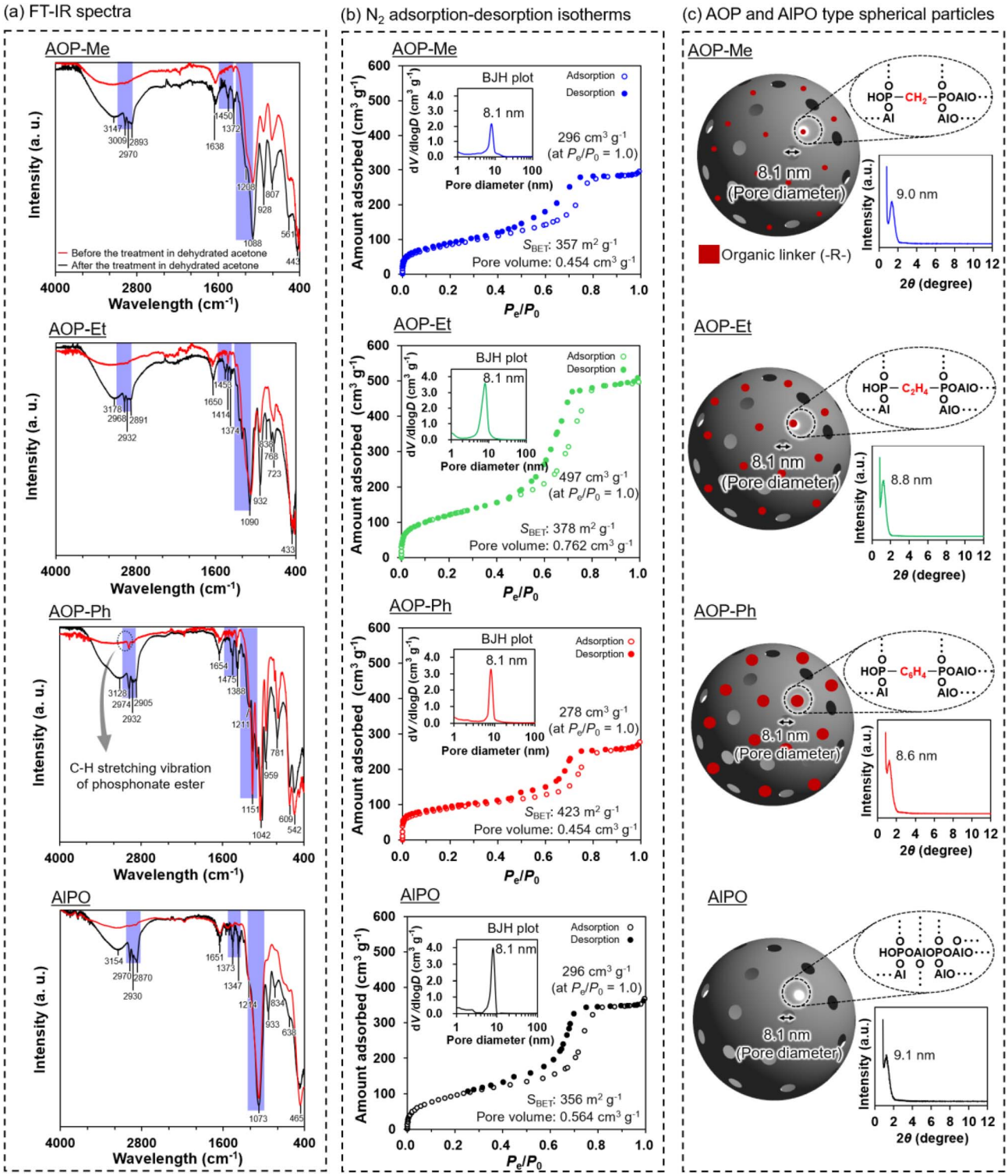

Fig. 1 Synthesis of mesoporous AOP and AlPO-type materials. (a) FT-IR spectra before and after treatment in dehydrated acetone, (b) N_2 adsorption–desorption isotherms and corresponding pore size distribution curves and (c) low-angle XRD patterns and schematic models of the porosity and framework structure for AOP-Me, AOP-Et, AOP-Ph and AlPO.

observed in the desorption branch, indicating the presence of very strong interaction of H_2O with the mesopore surfaces, especially ligation of H_2O molecules to the AlO_4 units and the hydrolysis of the AlPO-based frameworks.[12,39] According to the resultant surface hydrophobicity of AOP-Me as well as that observed for AlPO (H_2O-S_{BET}; 667 $m^2\ g^{-1}$ and 1.81), the H_2O-S_{BET} and H_2O-S_{BET}/N_2-S_{BET} values were still large (502 $m^2\ g^{-1}$ and 1.41). The adsorption capacity of AOP-Me (0.42 g g^{-1}, 93%

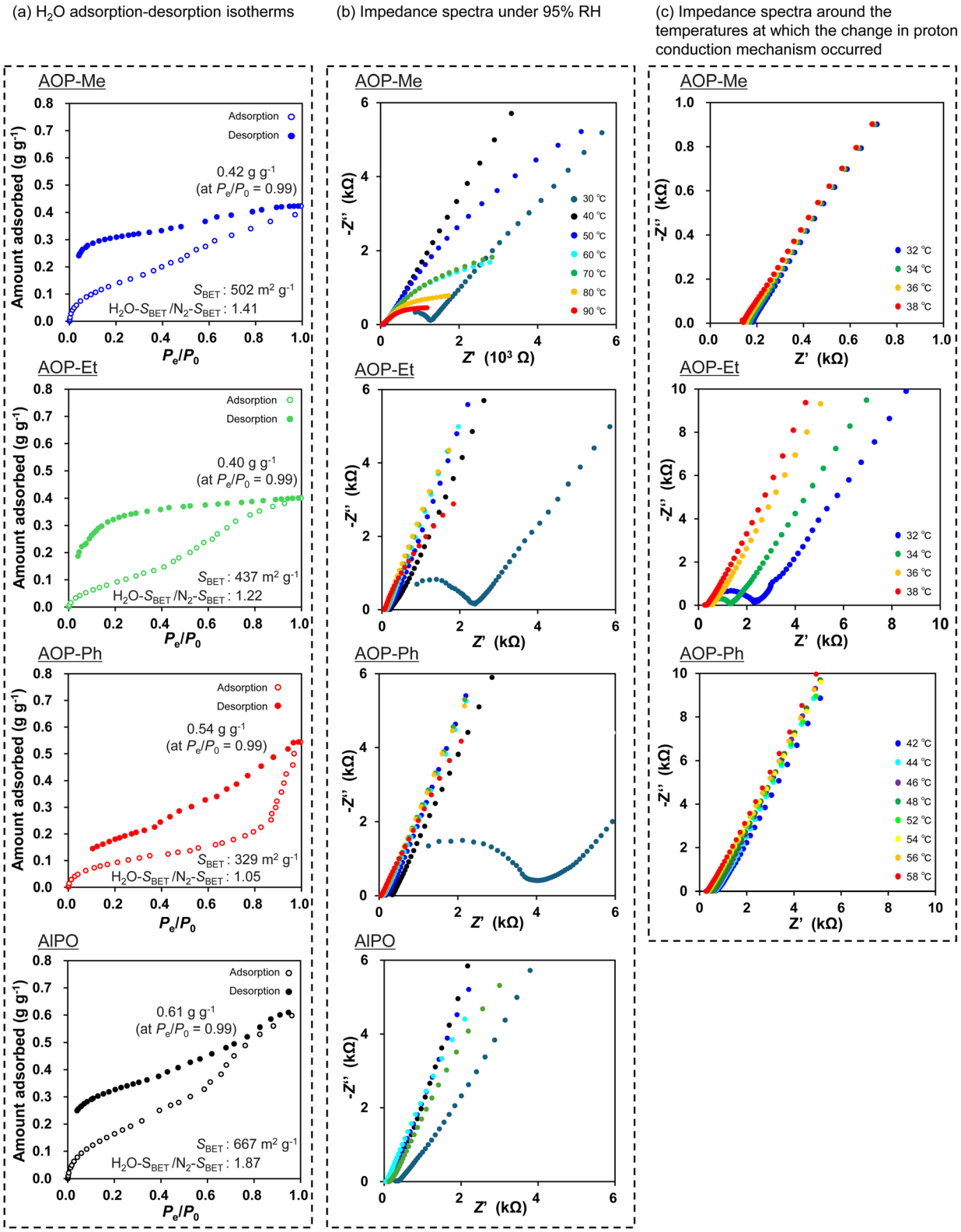

Fig. 2 Surface properties and proton conductivities of the mesoporous AOP and AlPO-type materials. (a) H_2O adsorption–desorption isotherms and (b and c) impedance spectra of disk-shaped pellets of AOP-Me, AOP-Et, AOP-Ph and AlPO under 95% RH at different temperatures and around the temperature at which the change in proton conduction mechanism occurred. Flattened semicircles in the high-frequency region contain two components, namely bulk and grain boundary resistance.[41]

of 0.45 $cm^3\ g^{-1}$ as the total pore volume) still arose from the hydrophilicity inside the mesopores and was almost comparable to that of AlPO (0.61 $g\ g^{-1}$, being more than the total pore volume of 0.56 $cm^3\ g^{-1}$). The adsorption behavior was changed by increasing the hydrophobicity of the organic linker (*e.g.*, AOP-Et and AOP-Ph). The H_2O-S_{BET} values of AOP-Et and AOP-Ph were respectively 437 $m^2\ g^{-1}$ and 329 $m^2\ g^{-1}$, suggesting a reduction in the average hydrophilicity due to the presence of $-C_2H_4-$ and many hydrophobic –Ph– groups throughout the frameworks. Accordingly, we can conclude that the order of the H_2O-S_{BET}/N_2-S_{BET}, AlPO (1.87) > AOP-Me (1.41) > AOP-Et (1.22) > AOP-Ph (1.05), is related to the surface properties of the frameworks.

The percentage of adsorbed H_2O per total pore volume (0.76 $cm^3\ g^{-1}$) decreased drastically to 53% (0.40 $g\ g^{-1}$) in the case of AOP-Et. However, due to an irregular uptake of H_2O in the region higher than $P/P_0 = 0.85$, the value (0.54 $g\ g^{-1}$ for AOP-Ph, 128% compared to the total pore volume of 0.42 $cm^3\ g^{-1}$) was probably overestimated. Considering the adsorbed amount at $P/P_0 = 0.86$ before the capillary condensation of AOP-Ph, H_2O molecules would be mainly captured inside the mesopores of AOP-type materials such as AOP-Me, AOP-Et and AOP-Ph, including AlPO. From this viewpoint, the surface properties of the AlPO-based frameworks can be successfully designed by incorporating organic groups showing different hydrophobicity. Such AOP-type mesoporous materials are then good candidates to evaluate proton conductivity derived from the surface properties of the AlPO-based frameworks. The uptake of H_2O can be changed sequentially according to the RH. After completing the desorption measurement (even at very low $P/P_0 < 0.05$), not all of the H_2O molecules were eliminated on the surfaces of all the mesoporous materials. This is due to the strong interaction of H_2O molecules with the AlO_4 units and/or acidic P–OH groups of the AlPO-based inorganic frameworks.[12,39,40] However, the residual H_2O molecules were removed and similar adsorption–desorption properties were recovered by a pretreatment that involved heating at 80 °C for 3 h under vacuum (see Fig. S4, as the 2nd cycle of H_2O adsorption–desorption measurement).

3.3 Proton conductivity of AOP-type mesoporous materials

The proton conductivity was initially measured for the series of AOP-Me, AOP-Et and AOP-Ph-type mesoporous materials, as well as the AlPO-type one, by using electrochemical impedance spectroscopy (EIS) under high-humidity conditions (95% RH) in the temperature range from 30 °C up to 90 °C. The resultant EIS are shown in Fig. 2b and c; the proton conductivity for each material is also listed in Table 1. The corresponding Arrhenius plots are shown in Fig. 3a–c, being crucial for analyzing the proton conductive mechanism by using the activation energy (E_a). The E_a value for AOP-Me was 4.4 eV below 32 °C (at $1000/T\ K = 3.28$), revealing that the proton conduction proceeded by the Vehicle mechanism.[20] The E_a value at the hydrophilic surfaces of the AlPO type frameworks was extremely low (0.38 eV), indicating that protons were transported by the Grotthuss mechanism.[20] These results suggest that the proton conduction mechanism at the surface of the AlPO-type frameworks is

Table 1 Proton conductivities of AOP and AlPO-type mesoporous materials under different humidity and temperature conditions

Conditions		Proton conductivity ($S\ cm^{-1}$)			
Humidity	Temperature	AOP-Me	AOP-Et	AOP-Ph	AlPO
50% RH	25 °C	1.62×10^{-6}	2.65×10^{-8}	1.77×10^{-8}	1.42×10^{-6}
60% RH		2.90×10^{-6}	6.42×10^{-8}	7.18×10^{-8}	1.59×10^{-6}
70% RH		4.67×10^{-6}	1.92×10^{-7}	2.64×10^{-7}	2.27×10^{-6}
80% RH		8.62×10^{-6}	5.59×10^{-7}	1.04×10^{-6}	5.59×10^{-6}
90% RH		1.72×10^{-5}	1.26×10^{-6}	4.51×10^{-6}	4.87×10^{-5}
95% RH	25 °C	2.49×10^{-5}	2.06×10^{-6}	1.03×10^{-5}	1.40×10^{-3}
	30 °C	3.74×10^{-4}	2.41×10^{-5}	2.05×10^{-5}	1.73×10^{-3}
	32 °C	1.38×10^{-3}	4.58×10^{-5}	—	—
	34 °C	1.44×10^{-3}	1.05×10^{-4}	—	—
	36 °C	1.58×10^{-3}	2.38×10^{-4}	—	—
	38 °C	1.67×10^{-3}	6.41×10^{-4}	—	—
	40 °C	1.78×10^{-3}	1.12×10^{-3}	1.29×10^{-4}	3.15×10^{-3}
	42 °C	—	—	1.68×10^{-4}	—
	44 °C	—	—	2.15×10^{-4}	—
	46 °C	—	—	3.02×10^{-4}	—
	48 °C	—	—	3.90×10^{-4}	—
	50 °C	2.32×10^{-3}	1.67×10^{-3}	5.33×10^{-4}	5.17×10^{-3}
	52 °C	—	—	7.16×10^{-4}	—
	54 °C	—	—	8.12×10^{-4}	—
	56 °C	—	—	8.69×10^{-4}	—
	58 °C	—	—	9.58×10^{-4}	—
	60 °C	3.05×10^{-3}	2.46×10^{-3}	1.04×10^{-3}	6.20×10^{-3}
	70 °C	3.55×10^{-3}	3.05×10^{-3}	1.24×10^{-3}	1.54×10^{-3}
	80 °C	4.57×10^{-3}	4.32×10^{-3}	1.73×10^{-3}	—
	90 °C	5.51×10^{-3}	5.72×10^{-3}	2.30×10^{-3}	—

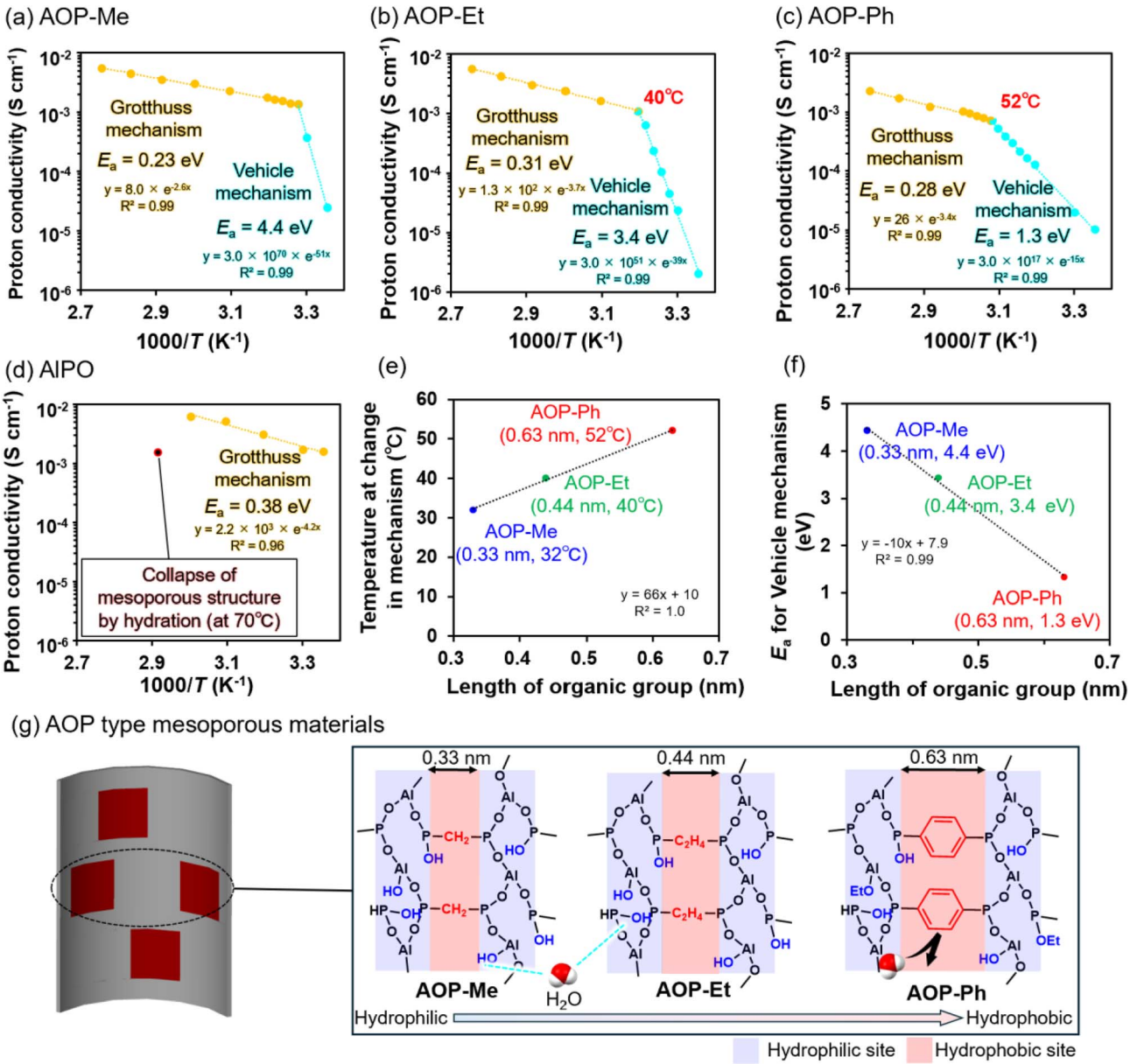

Fig. 3 Arrhenius plots of the proton conductivity for (a) AOP-Me, (b) AOP-Et, (c) AOP-Ph and (d) AlPO under 95% RH, the correlation between (e) the temperature at which the change in the proton conduction mechanism occurred and (f) the activation energy for the Vehicle mechanism and the length of the organic linkers, with (g) a schematic illustration of proton conduction by H_2O molecules at the surface of the AOP-type frameworks.

changed into the Vehicle mechanism by integrating hydrophobic organic groups. Protons are provided from P–OH and P=O groups at the surfaces around uniform mesopores and conducted with H_2O molecules adsorbed on the hydrophilic AlPO-type frameworks. In addition, due to the hydrated (hydrophilic) AlO_4 units at the surfaces of the mesopores,[12] the acidic coordinated H_2O may contribute to the proton supply. The length of the $-CH_2-$ linker (0.30 nm) is a little bit longer than that of the hydrogen-bond between the H_2O molecules (about 0.28 nm). This structural feature is quite important for avoiding the formation of a continuous network of hydrogen-bonded H_2O molecules. The proton conduction is limited by the Vehicle mechanism at low temperature (*e.g.*, 30 °C) and changed into the Grotthuss mechanism with an increase in temperature. Eventually, the proton conductivity of AOP-Me reached up to 5.51×10^{-3} S cm^{-1} at 90 °C.

The change in proton conduction mechanism was also observed for AOP-Et and AOP-Ph with an increase in temperature (see Fig. 3b and c). The proton conduction at the surface of AOP-Et below 40 °C (at $1000/T$ K = 3.19) occurred with the E_a value of 3.4 eV. The temperature at which the change in proton conduction mechanism occurred became higher in the presence of the $-C_2H_4-$ linker (0.44 nm), which was slightly longer than the $-CH_2-$ one (0.30 nm). Eventually, the proton

conductivity of AOP-Et was then 5.72×10^{-3} S cm^{-1} at 90 °C, being almost comparable to that observed for AOP-Me. The transformation in the proton conductive mechanism was also confirmed in the Arrhenius plot for AOP-Ph with a bulky organic group (–C_6H_4–, 0.63 nm) at temperatures higher than those observed for AOP-Me and AOP-Et. The E_a values were evaluated to be 1.3 eV and 0.28 eV below and above 52 °C (3.08 at 1000/T K), respectively. A continuous network of hydrogen-bonded H_2O molecules is possibly restricted at the surfaces of the AOP-type framework by the presence of a hydrophobic–Ph– linker. This is the main reason why the resultant proton conductivity of AOP-Ph, 2.30×10^{-3} S cm^{-1} at 90 °C, was slightly lower than those observed for AOP-Me and AOP-Et. As attached to Fig. 3e–g as a brief summary to illustrate the proton conduction over the AOP-type frameworks, the mean size of the organic linker is positively proportional to the temperature at which the change in proton conductive mechanism occurs and negatively proportional to the E_a value.

The E_a value of proton conduction by the Vehicle mechanism is related to the mobility of proton carriers (H_2O molecules).[42] In the AOP-type mesoporous materials, as the organic linker becomes longer, the proportion of hydrophobic organic groups on the pore surface increases. In contrast to the pure hydrophilic AlPO surfaces, the hydrogen-bonding of the H_2O molecules is possibly restricted by the presence of hydrophobic organic linkers to impede the transfer of H_2O molecules, resulting in a decrease of about 1 eV in E_a for every 0.1 nm increase in the length of the organic linker (see Fig. 3f). The FT-IR spectra of the AOP-type mesoporous materials were measured before and after standing at 30 °C and 95% RH for further understanding (see Fig. S5). Clear differences have hardly been found in the bands corresponding to O–H bonds in all the FT-IR spectra. Although pores smaller than 1 nm are necessary for complete destruction of the water structure, the surfaces of the AOP-type mesoporous materials, especially those near hydrophobic organic groups, strongly restrict the hydrogen-bonding of the H_2O molecules.[43] Accordingly, even in the case of AOP-type mesoporous materials, it is rational to consider that hydrophobic organic groups influence the hydrogen-bonding between the H_2O molecules near the mesopore surfaces, which contributes to the proton transfer from the proton donor group (–P–OH group) and the proton conduction between H_2O molecules. This knowledge demonstrates the possibility to control the proton/H_2O transfer rate and mechanism inside the mesopores of AOP-type materials by adjusting the organic linker.

The introduction of hydrophobic organic linkers (*e.g.*, –Ph–) was, however, useful for a drastic improvement in structural stability under the high RH conditions even at higher temperatures. The proton conductivity of the AlPO-type mesoporous material decreased from 6.20×10^{-3} at 60 °C down to 1.54×10^{-3} S cm^{-1} at 70 °C. This is caused by the collapse (hydrolysis) of the AlPO-type frameworks due to the presence of H_2O molecules at this level of humidity permeating and hydrolyzing the Al–O–P bonds. Interestingly, in the cases of AOP-type materials, especially AOP-Ph, the proton conductivity was maintained even under 95% RH at temperatures higher than 70 °C by enhancing the structural stability of the AOP-type frameworks through the presence of hydrophobic organic linkers that prevent H_2O molecules from contacting the surfaces of the AOP-type frameworks. The proton conductivities of AOP-Me and AOP-Et were higher than 5.0×10^{-3} S cm^{-1} at 90 °C and comparable to that of the AlPO-type mesoporous material before swelling by H_2O, resulting in them working as stable proton conductors for at least one week at 90 °C (see Fig. S6). Considering the operating conditions of general-purpose proton conductors at higher temperature to promote catalytic reactions, robust AOP-type mesoporous materials have the potential to overcome the lower stability of AlPO-based frameworks under high RH conditions and may be applied in practical uses as stable proton conductors.

The proton conductivity of each material was also measured by EIS at 25 °C under different RHs ranging from 50% to 95%, as shown in Fig. 4 and Table 1. The proton conductivity of AOP-Me, AOP-Et and AOP-Ph increased exponentially with RH, showing that the proton conduction proceeded by the Vehicle mechanism to transport protons by the direct movement of H_2O molecules. Although the proton conductivity of AlPO was also correlated exponentially under the conditions of 50–80% RH, as well as the AOP-type ones, its deviation was observed under conditions above 90% RH according to the Grotthuss mechanism based on the formation of the hydrogen-bonding of H_2O molecules at high RH (*e.g.*, 80–90%). To achieve higher proton conductivity under high RH (*e.g.*, 90%) even at low temperature (*e.g.*, 25 °C), an enhancement of the surface hydrophilicity is helpful for conducting protons effectively by the Grotthuss mechanism. Under medium RH (*e.g.*, 50–80%) at low temperature (*e.g.*, 25 °C), all proton conductions were however governed by the Vehicle mechanism. From this viewpoint, weak interactions with the surfaces of proton conductors lead to fast transportation of H_2O molecules inside the mesopores by the Vehicle mechanism. The amount of H_2O molecules inside the mesopores should be controlled by the precise design of the surface properties between hydrophilicity and hydrophobicity depending on the composition of the frameworks under low RH to avoid continuous networking of H_2O molecules inside the mesopores. Actually, several initiatives have reported that materials with extremely hydrophobic channels exhibited outstanding proton conductivity.[44,45]

Overall, proton conduction over AOP-type frameworks, including the AlPO-type one, can be categorized by the conditions with and without enough humidity. Under conditions with high humidity (95% RH), hydrophilic AlPO surfaces are advantageous for smooth proton conduction by the Grotthuss mechanism through the networking of H_2O molecules even at temperatures below 60 °C. Such proton conduction is reduced by the presence of hydrophobic organic linkers, but can be maintained (>10^{-3} S cm^{-1}) at temperatures above 70 °C by the presence of many H_2O molecules. However, the proton conductivity should be improved in practical uses, like Nafion showing a remarkable proton conductivity of 10^{-1}–10^{-2} S cm^{-1}.[46] In this case, the attachment of hydrophilic acidic groups (*e.g.*, –SO_3H) to hydrophobic organic linkers is promising for improving the mobility of protons at the surfaces of AOP-type frameworks, as well as the proton conductivity.[23] The use of organic linkers having heteroatoms such as amino

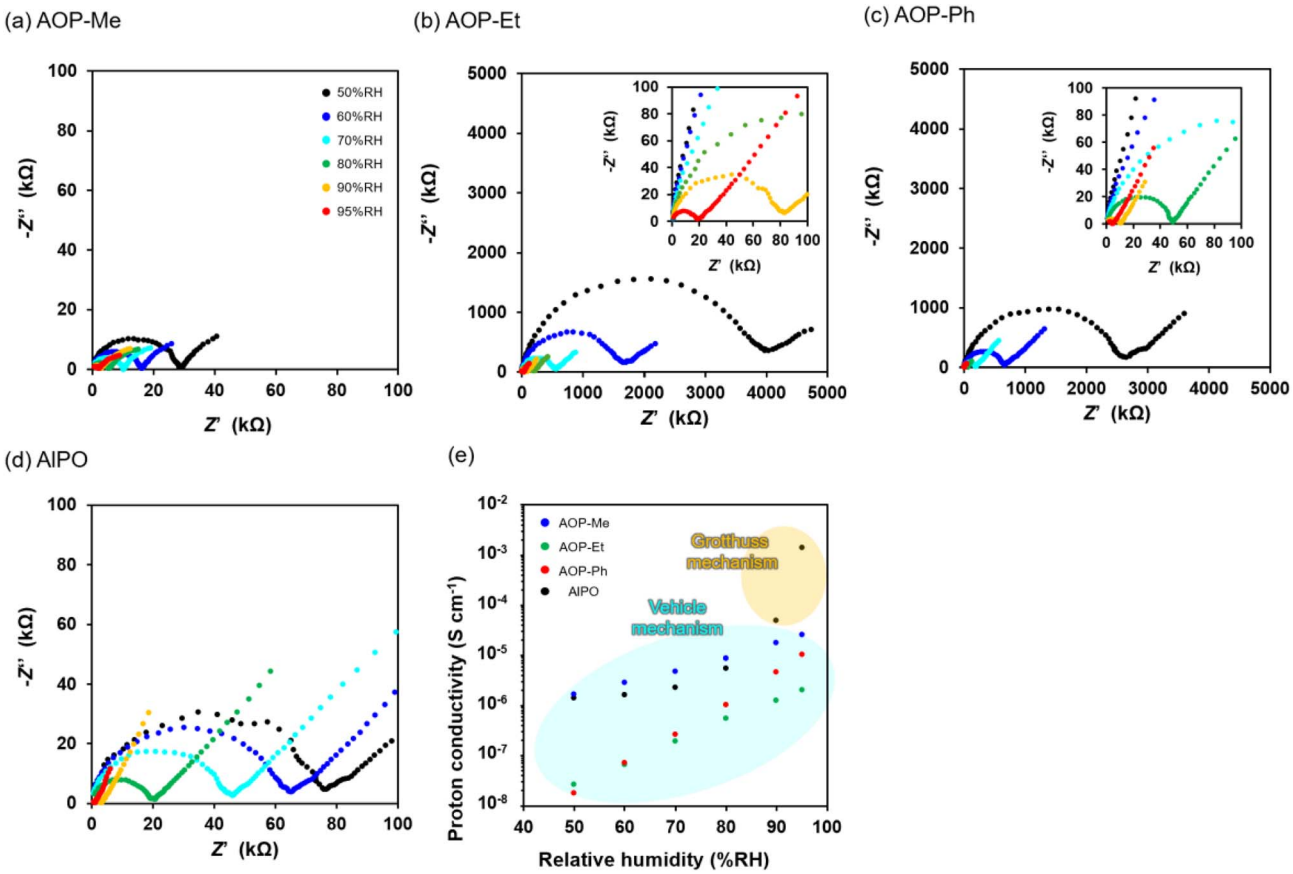

Fig. 4 Impedance spectra of the disk-shaped pellets of (a) AOP-Me, (b) AOP-Et, (c) AOP-Ph and (d) AlPO under different RH at 25 °C, with (e) the correlation between RH and proton conductivity of AOP and AlPO-type mesoporous materials.

groups (–NH_2) and heterocyclic rings is also useful for promoting the complete networking of H_2O molecules.[47,48] Under conditions with medium RH (*e.g.*, 50–80%), the amount of H_2O molecules inside the hydrophobic mesopores of AOP-type mesoporous materials is not enough for networking H_2O molecules, thereby leading to the change of the proton conduction mechanism into the Vehicle one considering the fact that a significant decrease in proton conductivity is confirmed even by using Nafion at low RH,[49] further design would be expected for improving the transport efficiency of H_3O^+ equivalent to the reduction of the conductive distance between H_2O molecules. For this purpose, the increase in hydrophobicity of the mesopore surface is only desirable without a decrease in the proton sources (*e.g.*, free phosphoric groups and hydrated (hydrophilic) AlO_4 units) inside the mesopores by such excessive enlargement of the organic linkers. The design of the molecular structure, *e.g.*, the addition of hydrophobic functional groups such as fluorine, is one of the possibilities for solving this problem (see Fig. S7).[44]

4. Conclusions

A series of AOP-type mesoporous materials showing surface properties between hydrophilicity and hydrophobicity due to the presence of organic linkers (*e.g.*, –CH_2–, –C_2H_4– and –C_6H_4–) at the molecular scale between the AlPO-like units was prepared for investigating proton conductivity at the hydrophilic AlPO surfaces. Under conditions with high humidity (*e.g.*, 95% RH) at low temperature (*e.g.*, 30 °C), hydrophilic AlPO surfaces without any organic linkers were advantageous for obtaining better proton conduction (1.73×10^{-3} S cm^{-1}) and AOP-type frameworks were not helpful for conducting enough protons. However, the proton conductivity at the AOP surfaces was comparable to that observed for the AlPO-type frameworks with an increase in temperature (*e.g.*, above 32 °C and 40 °C for small –CH_2– and –C_2H_4– and above 52 °C for bulky –C_6H_4–). This is because the formation of a continuous network of hydrogen-bonded H_2O molecules is disturbed by the presence of hydrophobic organic linkers at low temperatures and improved by increasing the temperature. Interestingly, proton conduction by the Vehicle mechanism was promoted very well at the strongly hydrophobic surfaces (*e.g.*, –C_6H_4–) showing a weak interaction with H_2O molecules. Although the proton conductivity of AOP-type mesoporous materials has not yet reached that of top-notch proton-conducting materials such as Nafion, their potential is comparable and/or superior to almost all inorganic and inorganic/organic hybrid materials (see Table S2). Although the development of AOP-type mesoporous materials as proton conductors is still in its infancy, our knowledge is important as a rational guide for designing AOP-based proton-conducting materials.

Author contributions

Takahiro Ami: methodology, investigation, formal analysis, data curation, writing – original draft, visualization; Kouki Oka: methodology, investigation, funding acquisition, resources, writing – review & editing; Hitoshi Kasai: supervision, resources; Tatsuo Kimura: conceptualization, methodology, investigation, writing – review & editing, validation, visualization.

Conflicts of interest

The authors declare no conflicts of interest.

Data availability

The data supporting this article have been included as part of the supplementary information (SI). Supplementary Information is available. See DOI: **https://doi.org/10.1039/d5ta06982c**.

Acknowledgements

This work was conducted with the partial support of the Cooperative Research Program "Network Joint Research Center for Materials and Devices (MEXT)". This work was also supported by the Japan Society for the Promotion of Science (JSPS) KAKENHI Grant Numbers 23K17945, 23H03827, 24K01552, and 24KJ1580. K. O. is grateful for support from the Environment Research and Technology Development Fund (JPMEERF20241RA4) of the Environmental Restoration and Conservation Agency provided by the Ministry of the Environment of Japan. K. O. also acknowledges support from Shorai Foundation for Science and Technology, TEPCO Memorial Foundation, Amano Industry Technology Laboratory, The Yamada Science Foundation, Kenjiro Takayanagi Foundation, Kansai Research Foundation for Technology Promotion, Yashima Environment Technology Foundation, JACI Prize for Encouraging Young Researcher, Foundation for Interaction in Science and Technology, Iketani Science and Technology Foundation, and Ichimura Foundation for New Technology.

References

1 Y. Nagao, *ChemElectroChem*, 2024, **11**, e202300846.
2 R.-T. Liu, Z.-L. Xu, F.-M. Li, F.-Y. Chen, J.-Y. Yu, Y. Yan, Y. Chen and B. Y. Xia, *Chem. Soc. Rev.*, 2023, **52**, 5652–5683.
3 M. B. Hanif, S. Rauf, Z. Abadeen, K. Khan, Z. Tayyab, S. Qayyum, M. Mosiałek, Z. Shao, C.-X. Li and M. Motola, *Matter*, 2023, **6**, 1782–1830.
4 J. Yu and R. Xu, *Chem. Soc. Rev.*, 2006, **35**, 593–604.
5 C. Zhang, Y. Yan, Z. Huang, H. Shi, C. Zhang, X. Cao and J. Jiang, *Inorg. Chem. Commun.*, 2018, **96**, 165–169.
6 J. Zhu, Y. Yan, J. Liu and X. Song, *Inorg. Chem. Commun.*, 2015, **56**, 133–136.
7 Y. Sun, Y. Yan, Y. Wang, Y. Li, J. Li and J. Yu, *Chem. Commun.*, 2015, **51**, 9317–9319.
8 Y. Mu, Y. Wang, Y. Li, J. Li and J. Yu, *Chem. Commun.*, 2015, **51**, 2149–2151.
9 K.-M. Zhang, M.-F. Ji, X.-Y. Zhou, F. Xuan, B.-Y. Duan, Y. Yuan, G.-X. Liu, H.-B. Duan and H.-R. Zhao, *RSC Adv.*, 2023, **13**, 12703–12711.
10 T. Kimura, *Microporous Mesoporous Mater.*, 2005, **77**, 97–107.
11 T. Kimura, Y. Sugahara and K. Kuroda, *Chem. Commun.*, 1998, 559–560.
12 T. Kimura, Y. Sugahara and K. Kuroda, *Microporous Mesoporous Mater.*, 1998, **22**, 115–126.
13 L. Wang, B. Tian, J. Fan, X. Liu, H. Yang, C. Yu, B. Tu and D. Zhao, *Microporous Mesoporous Mater.*, 2004, **67**, 123–133.
14 B. Tian, X. Liu, B. Tu, C. Yu, J. Fan, L. Wang, S. Xie, G. D. Stucky and D. Zhao, *Nat. Mater.*, 2003, **2**, 159–163.
15 J. W. Kriesel, M. S. Sander and T. D. Tilley, *Adv. Mater.*, 2001, **13**, 331–335.
16 Y. Ye, W. Guo, L. Wang, Z. Li, Z. Song, J. Chen, Z. Zhang, S. Xiang and B. Chen, *J. Am. Chem. Soc.*, 2017, **139**, 15604–15607.
17 D. J. Mann and M. D. Halls, *Phys. Rev. Lett.*, 2003, **90**, 195503.
18 R. Sahoo, S. Mondal, S. C. Pal, D. Mukherjee and M. C. Das, *Adv. Energy Mater.*, 2021, **11**, 2102300.
19 D.-W. Lim and H. Kitagawa, *Chem. Soc. Rev.*, 2021, **50**, 6349–6368.
20 X. Meng, H.-N. Wang, S.-Y. Song and H.-J. Zhang, *Chem. Soc. Rev.*, 2017, **46**, 464–480.
21 S.-S. Liu, Q.-Q. Liu, S.-Z. Huang, C. Zhang, X.-Y. Dong and S.-Q. Zang, *Coord. Chem. Rev.*, 2022, **451**, 214241.
22 B. N. Bhadra, I. Ahmed, H. J. Lee and S. H. Jhung, *Coord. Chem. Rev.*, 2022, **450**, 214237.
23 M. Furtmair, J. Timm and R. Marschall, *Microporous Mesoporous Mater.*, 2021, **312**, 110745.
24 L. Zhu, H. Zhu, L. Wang, J. Lei and J. Liu, *J. Energy Chem.*, 2023, **82**, 198–218.
25 K.-I. Otake and H. Kitagawa, *Small*, 2021, **17**, 2006189.
26 M. Rikukawa and K. Sanui, *Prog. Polym. Sci.*, 2000, **25**, 1463–1502.
27 T. Kimura, *Chem. Mater.*, 2003, **15**, 3742–3744.
28 T. Kimura, *Chem. Mater.*, 2005, **17**, 5521–5528.
29 A. Takamori and T. Kimura, *Langmuir*, 2023, **39**, 10680–10691.
30 D.-W. Lim and H. Kitagawa, *Chem. Rev.*, 2020, **120**, 8416–8467.
31 H. Xu, S. Tao and D. Jiang, *Nature Mater.*, 2016, **15**, 722–726.
32 T. Kimura, *Angew. Chem., Int. Ed.*, 2017, **129**, 13644–13648.
33 T. Kimura and Y. Yamauchi, *Chem. Asian J.*, 2013, **8**, 160–167.
34 M. R. Agliullin, I. A. Shamanaeva, A. R. Zabirov, V. V. Lazarev, V. N. Maistrenko and B. I. Kutepov, *Petrol. Chem.*, 2022, **62**, 291–300.
35 B. Mirtaheri, M. Shokouhimehr and A. Beitollahi, *J. Sol-Gel Sci. Technol.*, 2017, **82**, 148–156.
36 Y. Li, G. Chen, S. Zhu, H. Li, Z. Ma, Y. Liu and L. Liu, *Bull. Mater. Sci.*, 2019, **42**, 200.
37 Y. Shi, Z. Wang and J.-A. Zhou, *RSC Adv.*, 2018, **8**, 39214–39221.
38 M. A. Al-Ghouti and D. A. Da'ana, *J. Hazardous Mater.*, 2020, **393**, 122383.
39 T. Kimura, *Chem. Mater.*, 2005, **17**, 337–344.

40 A. Shigematsu, T. Yamada and H. Kitagawa, *J. Am. Chem. Soc.*, 2011, **133**, 2034–2036.
41 N. E. Wong, P. Ramaswamy, A. S. Lee, B. S. Gelfand, K. J. Bladek, J. M. Taylor, D. M. Spasyuk and G. K. H. Shimizu, *J. Am. Chem. Soc.*, 2017, **139**, 14676–14683.
42 K.-D. Kreuer, A. Rabenau and W. Weppner, *Angew. Chem., Int. Ed.*, 1982, **21**, 208–209.
43 A. Srivastava, S. Abedrabbo, J. Hassan and D. Homouz, *Sci. Rep.*, 2024, **14**, 15480.
44 T. Ami, K. Oka, S. Kitajima and N. Tohnai, *Angew. Chem., Int. Ed.*, 2024, **63**, e202407484.
45 K.-I. Otake, K. Otsubo, T. Komatsu, S. Dekura, J. M. Taylor, R. Ikeda, K. Sugimoto, A. Fujiwara, C.-P. Chou and A. W. Sakti, *Nature Commun.*, 2020, **11**, 843.
46 G. Zhao, H. Zhao, X. Zhuang, L. Shi, B. Cheng, X. Xu and Y. Yin, *J. Mater. Chem. A*, 2021, **9**, 3729–3766.
47 B.-X. Han, Y.-F. Jiang, X.-R. Sun, Z.-F. Li and G. Li, *Coord. Chem. Rev.*, 2021, **432**, 213754.
48 S. Wang, H. Luo, X. Li, L. Shi, B. Cheng, X. Zhuang and Z. Li, *Int. J. Hydrog. Energy*, 2021, **46**, 1163–1173.
49 S. Paddison, *Annu. Rev. Mater.*, 2003, **33**, 289–319.